American Mineralogist, Volume 74, pages 780–796, 1989

In situ deformation of micas: A high-voltage electron-microscope study

ANNEMARIE MEIKE
Materials and Chemical Sciences Division, Lawrence Berkeley Laboratory, University of California, Berkeley, California 94720, U.S.A.

ABSTRACT

Muscovite ($2M_1$) and biotite ($1M$) were sheared in situ at room temperature in a 1500-kV transmission electron microscope. The resultant activation of dislocations represents the first success of such an experiment in a rock-forming mineral. Only basal slip was activated in either mica, but the dislocations could be distinguished on micromechanical grounds that may be related to a macroscopic difference in ductility. Invariably, dislocations in the muscovite specimens activated with greater difficulty, despite the greater abundance of precipitates in the biotite specimens. Muscovite basal dislocations were long and roughly linear, oriented along [100] or [110]. They activated in short steps that advanced parallel to the dislocation line, a manner typical of screw dislocations. In contrast, biotite basal dislocations were curvilinear and advanced perpendicular to the dislocation line in bowed segments, characteristic of edge dislocations. The division of dislocation lines, often separated by areas of either reversed contrast or moiré fringes, was interpreted as dislocation dissociation. Dissociation appeared to facilitate obstacle circumvention in biotite. The proposed explanation for the micromechanical differences is based on the distribution of Peierls potential energy in the basal glide plane and other energy-minimization arguments. The agreement between the proposed model and observation suggests that the micromechanical difference is structurally determined by the octahedral layer. The proposed Peierls stress control of dislocation activity could be evaluated from natural evidence, based on an expected inverse relationship between the magnitude of the micromechanical differences and temperature.

INTRODUCTION

As similar studies of metals (e.g., Imura and Hashimoto, 1977; Richter, 1979) have already demonstrated, our knowledge of mineral micromechanics could benefit considerably from observations of deformation made in situ in the electron microscope. In situ experiments require meticulous preparation and are difficult to interpret. However the ability to observe, first hand, the fundamental interactions of dislocations has permitted significant advances in the fields of material strength, plasticity, and fracture in metals. The greater penetration of the high-voltage electron microscope (HVEM) over conventional microscopes is especially significant since it allows the use of thicker specimens, which produce behavior more like a bulk sample than the thinner foils. In view of these advantages, the potential applications to geologic materials are extensive and varied. The long-term goal of the present in situ experiments has been to determine values of dislocation activation stress in brittle rock-forming minerals. However, first it has been necessary to adapt standard techniques that were originally developed for metals to accommodate physical characteristics common to rock-forming minerals. These first experiments have been developed for the relatively flexible and easily prepared micas. Both muscovite and biotite were deformed to explore suggested distinctions in their deformation behavior (Bell and Wilson, 1981). The purpose of this paper is to describe preliminary results of dynamic deformation experiments and to discuss a possible energetic basis for the observed differences in dislocation activity between muscovite and biotite.

EXPERIMENTAL DETAILS

Specimens were taken from single crystals of biotite and muscovite, identified as $1M$ and $2M_1$, respectively, on the basis of systematic absences of reflections from the first- and higher-order Laue zones. Provenance and a detailed chemical anlaysis were not determined and were unnecessary for the purpose of this study. Thin layers (50–100 μm) of each type of mica peeled along (001) cleavage planes, also the softest slip system in the micas (Mügge, 1898), produced the most coherent specimen. The chosen specimen orientation also optimized image contrast for basal dislocations, but the standard tensile stage (Fig. 1) would produce no shear in that plane. Consequently, the straining geometry was modified through an intermediate sliding metal cage (Meike, 1988). Each end of the specimen could be attached to the cage pieces in a manner that allowed simple shear in the plane of the specimen and parallel to the tensile axis of the straining

0003–004X/89/0708–0780$02.00

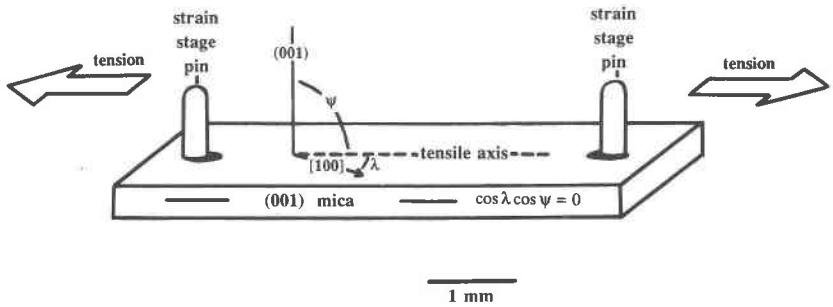

Fig. 1. A diagram that illustrates the absence of shear stress resolved onto the specimen plane in a standard tensile apparatus. The pins of the straining stage are attached through the circular holes at either end of the specimen.

stage (Fig. 2). As a result of this modification, the layers of mica could be oriented to maximize the potential for slip in the (001) glide plane. Narrow strips (~2 mm × ~5 mm) were cut from the mica layers such that one of the slip directions [110], [$\bar{1}$10], or [100] (Etheridge et al., 1973), determined between crossed polarizing filters or with percussion figures, was aligned with the long axis of the strip. The specimen was attached to the cage, and subsequently, a small (~1–2 mm) atom-milled (Franks, 1984) hole was opened in the middle of the viewing area for observation with the HTEM.

The experiments were conducted at room temperature using the Kratos 1500-kV high-voltage electron microscope (HVEM), at the National Center for Electron Microscopy, Lawrence Berkeley Laboratory. Unlike a conventional 100- or 200-kV microscope, the HVEM allowed the observation of thicker specimens, which reduced surface effects and the tendency of the specimen to fracture. The tensile stage was not equipped with stress- or strain-rate gauges, which would have been of little use since the dislocations activated at local stress concentrations. In the future, more accurate stress values will be obtained from dislocation-line-tension methods (Orowan, 1954; Messerschmidt and Appel, 1979; Gerold, 1983). The tensile stage was fitted with a motor drive and a set of piezoelectric crystals that separated pins attached to either end of the specimen-cage assembly. According to Campany et al. (1976), the expansion of the piezoelectric material at the maximum working potential (4.3 kV) translates an extension of roughly 8 μm to the specimen. In practice, the potential was increased slowly to a maximum of 3 kV. The voltage was then removed, and the strain was compensated with the motor drive before the piezoelectric strain was continued. This procedure allowed maximum control over dislocation activity. Dislocations activated to a greater extent before fracture when the specimen was aged below the elastic limit. A successful deformation experiment lasted 4 to 6 h.

The experiments were recorded with a high-resolution video camera mounted below the viewing screen of the microscope. Observation centered around the stress raiser at the atom-milled perforation in order to improve the

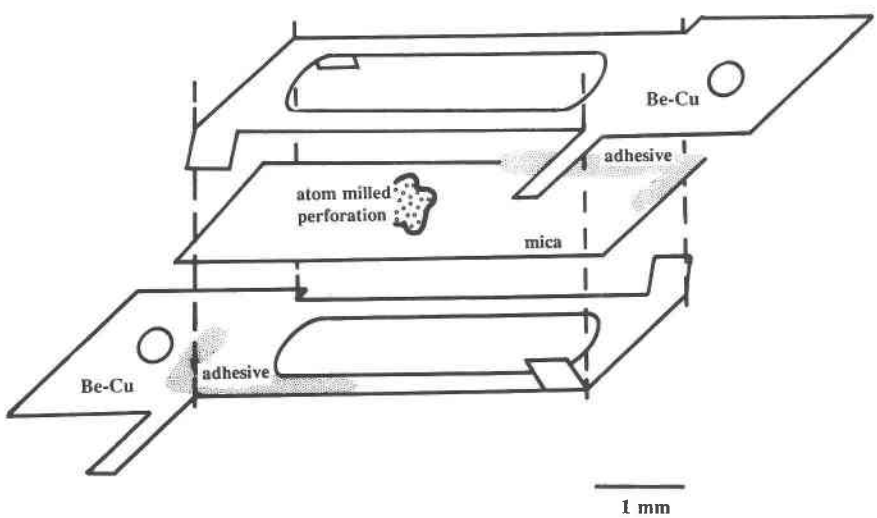

Fig. 2. An expanded diagram of the specimen-cage assembly for simple shear in the plane of the specimen. The pins of the straining stage are attached through the circular holes of the Be-Cu end pieces. The specimen is viewed through the ovoid aperture and near the atom-milled edge.

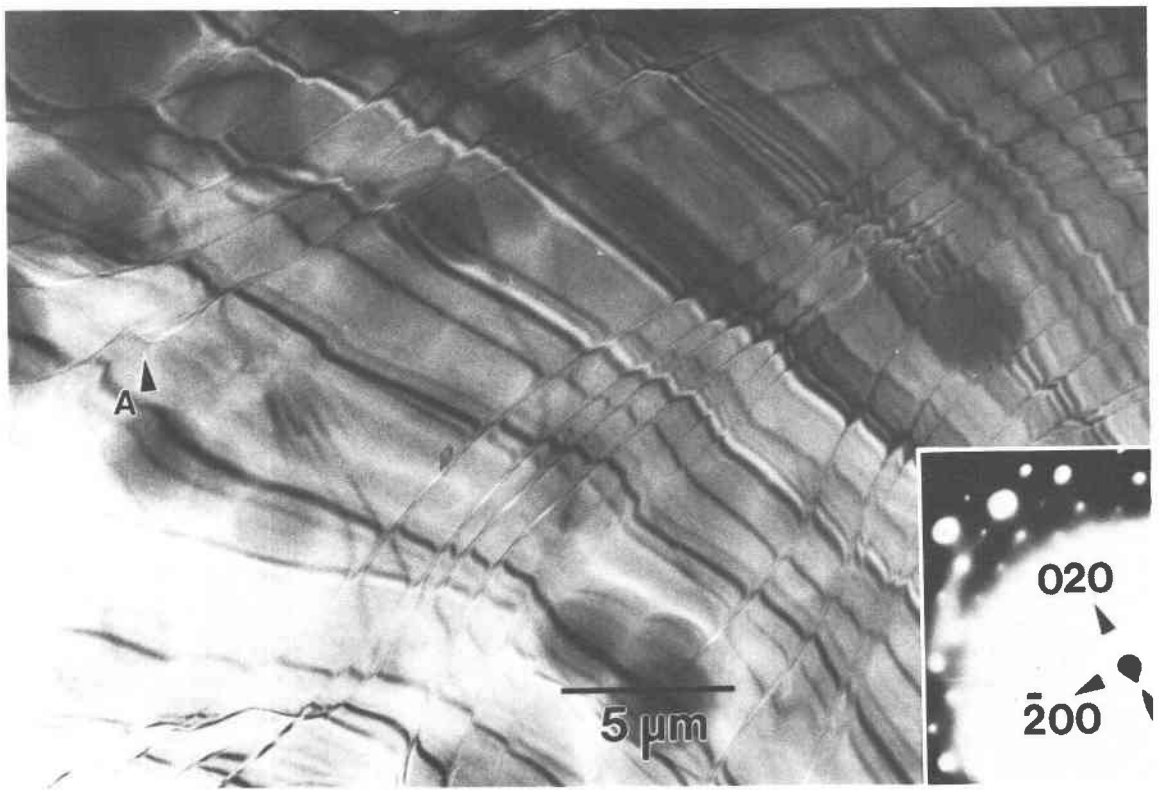

Fig. 3. A bright-field photomicrograph of a typical muscovite specimen; virtually free of precipitates and defects other than long, straight [100]- and [110]-oriented basal dislocations. When activated, the steps become more arcuate (arrow A).

chance of recording dislocation activity on videotape. Standard static photomicrographs were recorded at intervals throughout each straining sequence to obtain both images that were free of mechanical vibrations and diffraction patterns that were too intense to record with the sensitive video camera. During the experiment, specimen orientation could be maintained to some extent with double-axis tilt controls. Nevertheless, specimen rotation and bending caused changes in image contrast that could have been interpreted as dislocation activation. Three major causes of apparent dislocation motion were (1) the movement of Bragg, moiré, and thickness fringes, (2) the apparent relative motion of stationary dislocations with respect to moving fringes, and (3) the disappearance of dislocations rotated into a low-contrast orientation. Tilting experiments were performed between deformation episodes in order to locate low contrast dislocations. In addition, the videotapes were reviewed repeatedly in an effort to establish the relative movement of dislocations with respect to stationary reference points such as precipitates or an edge of the sample.

The character of the dislocations was verified when possible under static conditions using image-contrast analysis. The crystal was tilted from the symmetrical [001] orientation to positions in which one reflection dominated (called "two-beam" conditions). The intent of these experiments was to identify reflections for which the dislocations showed the least contrast, for comparison to predicted invisibility conditions for each of the possible Burgers vectors (Van der Biest and Thomas, 1976). The achievement of perfect two-beam conditions in mica could be difficult, because the $hk0$ reflections were closely spaced. Usually the diffraction pattern can be used to evaluate the accuracy of the two-beam assumption. However, dark bands (bend contours) in the images indicated that the crystals were bent and that the diffraction pattern applied strictly to a very small portion of the image. Fortunately, the bend contours could be used to an advantage. Each contour could be indexed according to the corresponding reciprocal space reflection, and the effects of a number of reflections could be compared within a single image.

Observations

Muscovite

The muscovite specimens were virtually free of precipitates. The only defects present were dislocations in the (001) glide plane. These long and fairly straight [100]- and [110]-oriented dislocations were offset within the glide plane by short steps (Fig. 3) and were difficult to activate. The term "step" refers to a short displacement of the

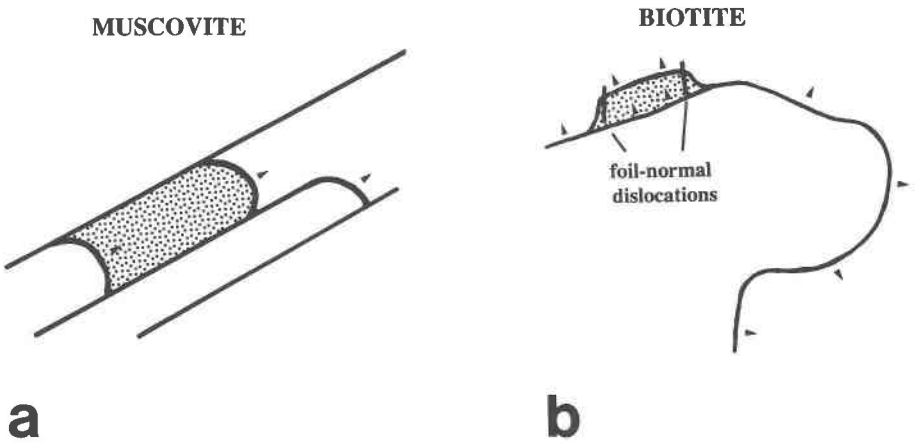

Fig. 4. Diagrams of dislocation activation observed in muscovite and biotite. Arrows indicate the direction of dislocation motion. (**a**) The advance of a step parallel to a dislocation line, typical of screw dislocation glide. In this illustration, the dark line has split, and an area of reversed contrast separates the advancing and the trailing dislocation. (**b**) The passage of a dislocation around an obstacle by dissociation.

dislocation line within a single slip plane. When activated, the steps became more arcuate (Fig. 3, arrow A) and advanced continuously, parallel to the [100]- and [110]-oriented segments. Figure 4a illustrates this activation, which is typical of screw dislocation glide constrained only by Peierls stress (Nabarro, 1967, p. 188). Still photographs taken from a videotape of dislocation activation in muscovite (Fig. 5) document the slow advance of the stepped segments 1, 2, and 3, approximately 2 μm during the course of 1 min. The dark spot in the lower right corner can be used as a reference point in this sequence. The elapsed time in this and all other videotaped sequences is indicated in that corner. Frequently a line of dark contrast remained in place as the stepped segment advanced parallel to the dislocation line (Fig. 4a). The areas swept by the advancing dislocation segment could display both unchanged and reversed image contrast. For example, the reversed contrast in the area that steps 1 and 2 traversed (Fig. 5), was absent from the area that step 3 traversed.

Tilting experiments were conducted in both micas to determine the character of the dislocations. Selected bright-field images illustrate these experiments in muscovite (Fig. 6). The arrows (Figs. 6a–6d) indicate a common reference point. The wide dark bands visible in all of the images and indexed in Figure 6c represent bend contours. The image within the bend contour corresponds to the value of the reflecton (**g**): the dark central region in Figure 6a ($\mathbf{g} = 1\bar{3}0$), the dark diagonal band in Figure 6b ($\mathbf{g} = 1\bar{1}0$), and the wide dark band in Figure 6d ($\mathbf{g} = 020$). Three bend contours, $\mathbf{g} = 110$ (A), $\mathbf{g} = 020$ (B), and $\mathbf{g} = 1\bar{1}0$ (C) are marked in Figure 6c, but $\mathbf{g} = 200$, which dominated in the diffraction pattern, is outside the field of view. The dislocations, most of which have strong contrast for $\mathbf{g} = 1\bar{3}0$ (Fig. 6a), tended to favor either the [100] or the [110] orientation. The images of some lines intersect, but the presence of one line did not seem to affect the other. The [110]-oriented dislocation lines are best represented in the upper left corner of the photomicrographs. The lines were least visible for $\mathbf{g} = 1\bar{1}0$ (Fig. 6b). For the same reflection, however, bands of reversed contrast appeared between the [110] lines in the uppermost corner. Most of the [100]-oriented dislocations, best represented in the lower left side of the photomicrographs, were in strong contrast for $\mathbf{g} = 1\bar{3}0$ (Fig. 6a). Careful inspection suggested that three classes could be distinguished. The first class was visible in all of the images except for $g = 1\bar{1}0$ (Fig. 6b). A second class could be distinguished from the first by its invisibility for $\mathbf{g} = 1\bar{3}0$. A third class exhibited weak contrast for $\mathbf{g} = 1\bar{1}0$ (Fig. 6b) and low contrast for $\mathbf{g} = 020$ (Fig. 6d). The latter two classes of dislocations were associated with [100]-oriented bands of reversed contrast for $\mathbf{g} = 020$ (Fig. 6d).

Biotite

Compared to muscovite, basal slip in biotite was easier to activate and achieved much higher velocities, even though the biotite specimens contained more potential obstacles to dislocation motion. The dislocations were curvilinear (Figs. 7 and 8) and advanced in bowed segments perpendicular to the dislocation line, a manner typical of edge dislocations. A sequence of photographs taken from videotapes illustrates dislocation activation in biotite (Fig. 9). The sequence documents the motion of one dislocation (arrowed) that moved 1 μm in 3 s. The actual activation took place as a series of much more rapid jumps interspersed by periods of immobility. The image of the line appeared diffuse (Fig. 9b). After stress was released (Fig. 9c) and the dislocation returned to a former position, a loop appeared to have remained (Fig. 9d, arrow C) at the apogee of the advance.

When confronted by an obstacle, primarily planar and linear defects normal to the foil (Fig. 7), biotite dislocations frequently split into two lines separated by a 0.1- to

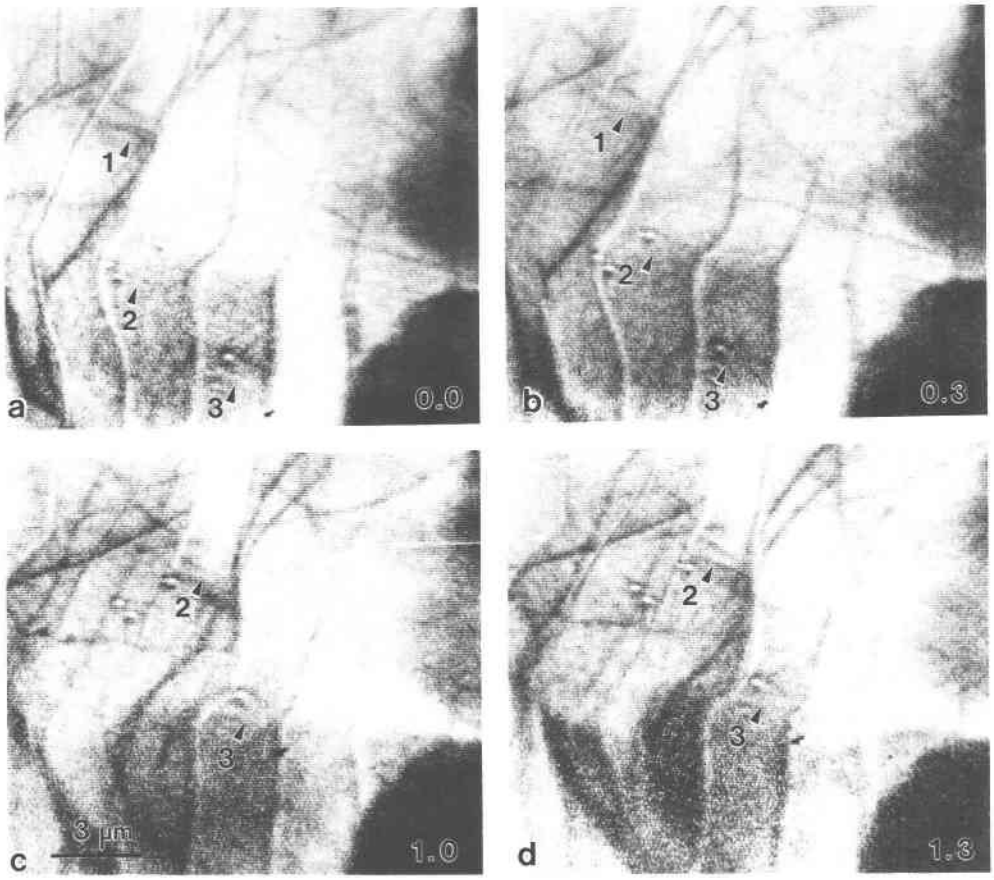

Fig. 5. Bright-field sequence (**a**, **b**, **c**, **d**) photographed from a videotape of dislocation activation in muscovite. Elapsed time is indicated in minutes at the lower right-hand corner, superimposed upon a dark area whose position can be used to measure the dislocation's advance. The step segments (1, 2, 3) moved continuously parallel to the dislocation line, approximately 2 μm in 1 min. Steps 1 and 2 change the contrast of the area that they traverse, but step 3 does not.

0.5-μm-wide region of reversed contrast. Basal plane dislocations curved outward from the foil-normal planar defects (Fig. 7, arrow B). The intersection between the basal dislocations and the planar defects appeared to have a steplike form. The foil-normal dislocations did not appear to be activated, and only slightly impeded basal slip. One videotaped episode documents a separation of a dislocation between two foil-normal dislocations, roughly 0.2 μm apart. The advancing line reversed the image contrast in an area at least 0.1 μm wide before it was rejoined by the trailing dislocation line. A diagram of the event, which occurred too quickly to record from videotape, is represented in Figure 4b. In another videotaped segment (Figs. 10a–10d), a dislocation line seemed to split, leaving an area of reversed contrast between, as it attempted to circumvent a large precipitate (~5–6 μm). Arrow A (Fig. 10b) indicates the original (0.0 min) location of the dislocation line. As it split, the dislocation wrapped slowly around the precipitate. Compared to the other observations of biotite, this advance was uncharacteristically slow, but beyond a critical radius (~4 μm), it attempted to neck rapidly. In this case, the Orowan mechanism (Orowan, 1954, p. 131) was unsuccessful because the limit of the strain stage was reached. However, concentric loops about precipitates and foil-normal dislocations (Fig. 8) were often observed in biotite after a deformation episode. Tilting experiments failed to reveal the radical changes in spacing one would expect if these concentric loops were thickness fringes due to pits in the specimen. Biotite sometimes displayed moiré fringes between the separated dislocation lines. These regions were often wider than those that displayed reversed contrast and did not appear to be associated with the passage of obstacles. Figure 7 (A arrows) illustrates moiré fringes observed within two concentric dislocation loops.

Discussion

The discussion below is divided into two parts. First, the observed differences in dislocation activity are considered in the context of the distribution of the Peierls potential energy in the basal plane of the two mica structures. The second part discusses the present interpretations of image contrast that will provide a working hypothesis for future experiments. Imaging conditions were

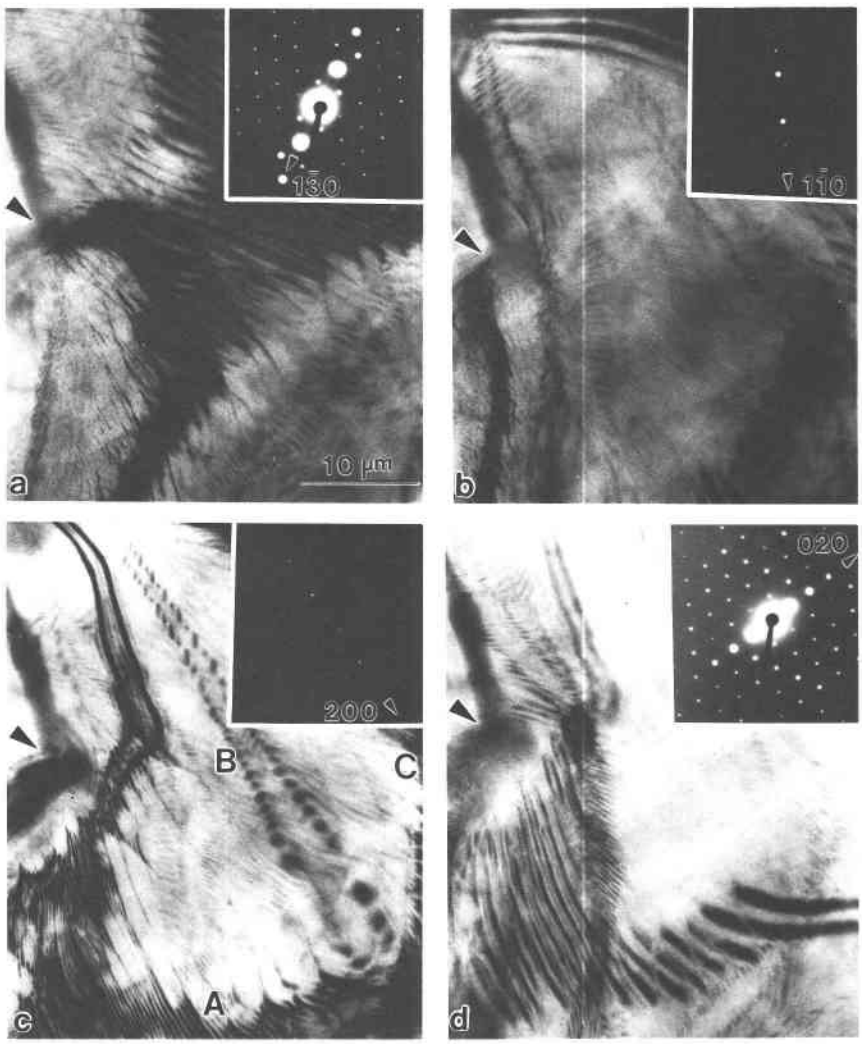

Fig. 6. Selected bright-field images from tilting experiments in muscovite. The arrows serve as reference points. Comparison of the contrast in these images with the predicted values in Tables 2 and 3 suggests that all the dislocations have screw character and that some are dissociated. (**a**) $\mathbf{g} = 1\bar{3}0$ corresponds to the central dark region. (**b**) $\mathbf{g} = 1\bar{1}0$ corresponds to the diagonal dark bend contour. (**c**) The bend contours that correspond to $\mathbf{g} = 110$ (A), $\mathbf{g} = 020$ (B), and $\mathbf{g} = 1\bar{1}0$ (C) are marked. (**d**) $\mathbf{g} = 020$ corresponds to the central wide dark band.

not easy to control in these dynamic experiments. The Burgers vector determinatons and the identification of partial dislocaton contrast are standard, but frequently could not be pursued rigorously. The resultant uncertainties were minimized by finding agreement among a combination of techniques. Therefore, the analytical methods are discussed in detail as applied to the micas and in the context of these dynamic experiments.

Crystal structure and Peierls stress

Muscovite and biotite are similar when viewed parallel to the *b* axis. Both structures are composed of octahedrally coordinated cations sandwiched between opposed, tetrahedrally coordinated silicate layers. For charge neutrality, Al occupies only ⅔ of the octahedral sites (dioctahedral) of muscovite, but Fe and Mg fill all the octahedral sites (trioctahedral) of biotite. The fundamental unit cell (multilayer) (Fig. 11a) can be stacked in a variety of ordered polytypic sequences that involve translations of $a/3$ and rotations of $30°n$ (where n is an integer). The arrangement of apical oxygens of a tetrahedral layer (Fig. 11b) illustrates the dioctahedral distortions caused by the vacant octahedral sites. The apical oxygen layer is used below as a reference, but does not imply that the dislocation is located in the octahedral layer. The Al atoms also shift at an angle to (001) that results in a slight corrugation in the [001] direction (e.g., Bailey, 1984). For lack of evidence to the contrary, the ordered (tetrahedral site) substitutional corrugation (Abbott and Burnham, 1988) is assumed to have an equivalent effect on muscovite and biotite structures.

The potential energy of a dislocation, called the Peierls

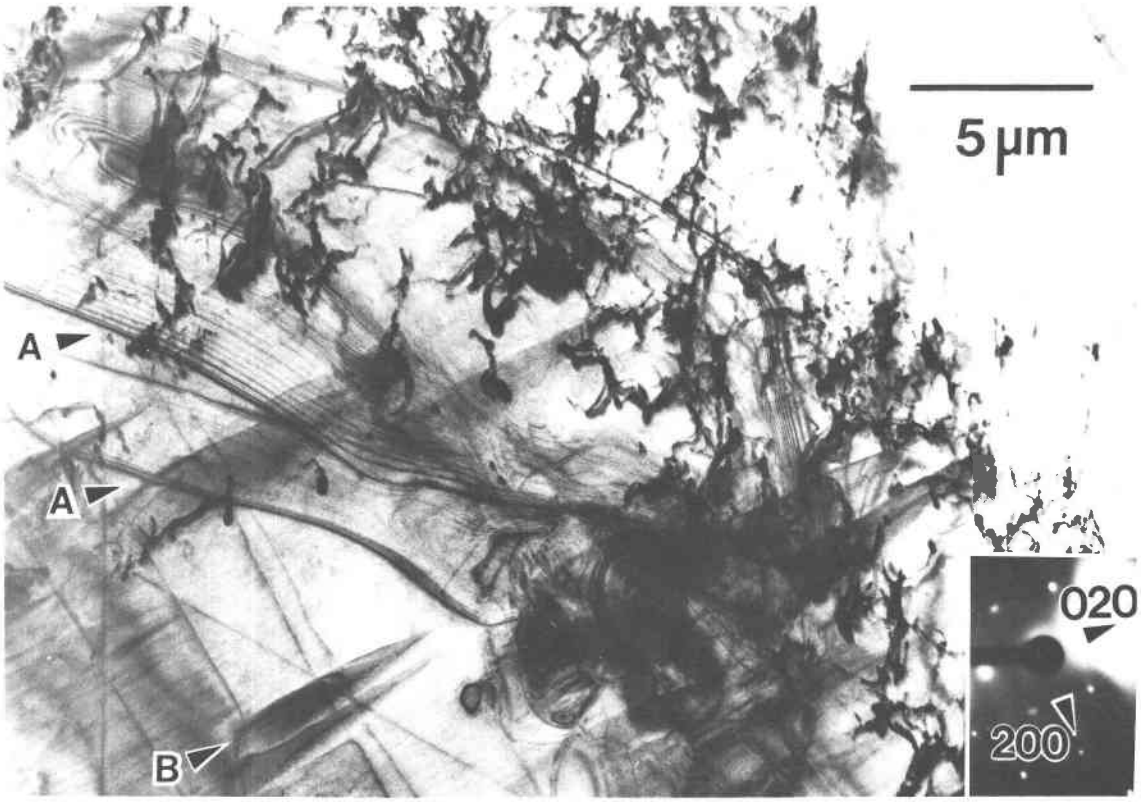

Fig. 7. Bright-field image of foil-normal planar (arrow B) and linear defects in biotite. Moiré fringes are visible within two of the concentric dislocation loops (arrows A).

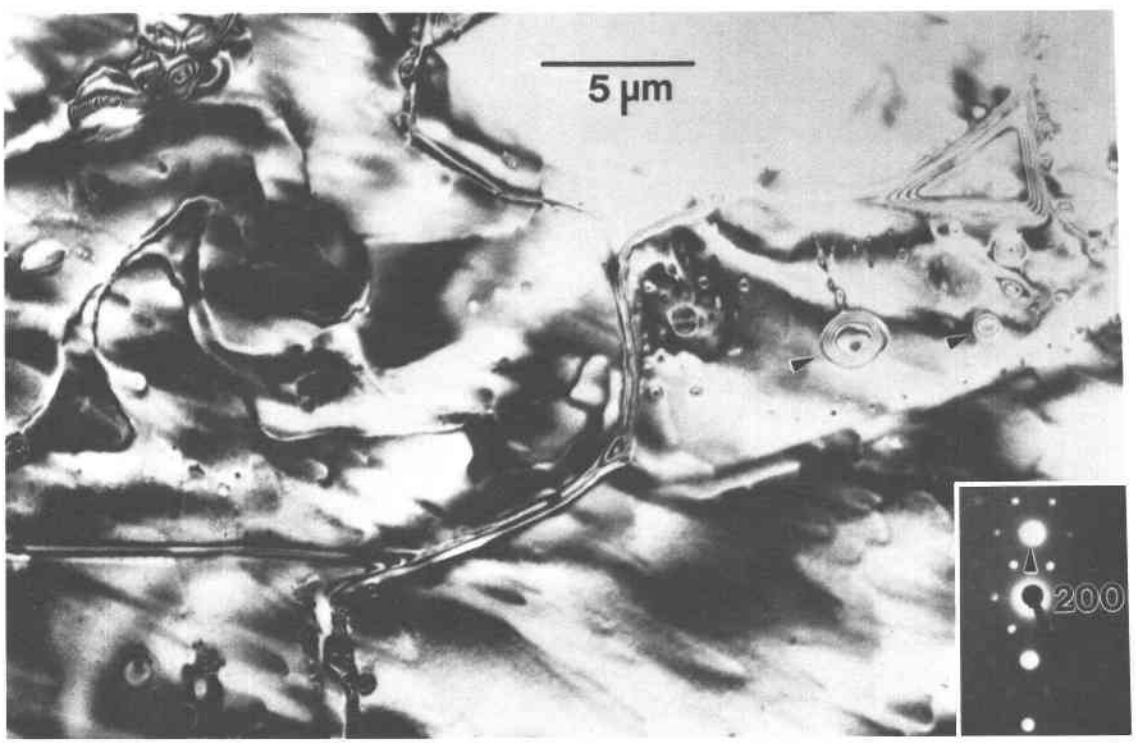

Fig. 8. The bright-field photomicrograph of biotite illustrates curvilinear dislocations in the (001) glide plane. The concentric loops about obstacles (arrows) are consistent with the successful operation of the Orowan mechanism.

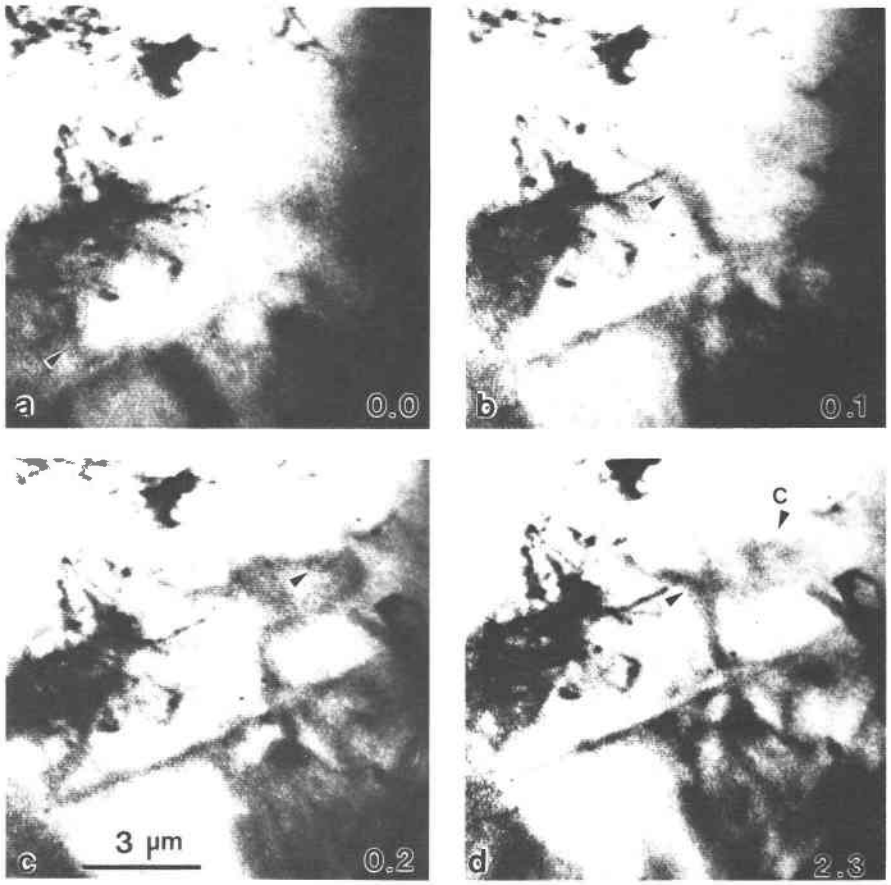

Fig. 9. Bright-field sequence photographed from a videotape of dislocation activation in biotite. Elapsed time is indicated in minutes at the bottom right. The dislocation's advance can be estimated relative to the precipitates. (**a–b**) The dislocation (arrows) makes short rapid advances in bowed segments perpendicular to the dislocation line. (**c–d**) The dislocation relaxes to an earlier position after stress is released, apparently leaving a loop (arrow C) behind. The diffuse image may be due to the depth of the dislocation in the foil. However, it is also probable that these dislocations are dissociated.

stress, is determined by the position of the surrounding atoms and thus fluctuates with the period of the lattice. The lowest Peierls stress position is located midway between planes of high atomic density (see discussions by Peierls, 1940; Frank and van der Merwe, 1949). One also would expect an unstressed dislocation line to align itself with the widest trough in the Peierls potential-energy surface and, consequently, the widest interplanar spacing. Examination of the trioctahedral layer suggests that the widest interplanar spacings are found along the symmetrically equivalent [100], [110], or [$\bar{1}$10] directions (Fig. 12a). Consequently, a dislocation influenced by a trioctahedral sheet favors those orientations equally. The *1M* biotite polytype stacking sequence, which involves a translation ($a/3$), does not affect the assessment of the dislocation orientation in biotite (Fig. 12b). The dioctahedral layer has a wider interplanar spacing in the [110] orientation than in the [100] or [$\bar{1}$10] orientations. Corrugations in the [001] direction would reinforce the tendency for a dislocation influenced by a dioctahedral layer to take up a [110] orientation (Fig. 12a). However, a [110] orientation is equivalent to [100] in the adjacent layer (Fig. 12b), since alternate layers of the $2M_1$ muscovite polytype are translated $a/3$ and rotated 30°.

The orientation of the dislocation line with respect to the Burgers vector establishes the screw or edge character of the dislocation. A Burgers vector is defined as a translation that closes the unit-cell circuit that has been disrupted by a dislocation. A complete Burgers vector (**b**) involves a translation to an equivalent lattice position. In biotite, the shortest translations to equivalent positions are $\mathbf{b} = \frac{a}{2}[110]$, $\frac{a}{2}[\bar{1}10]$, and $a[100]$ (Fig. 13). The shortest translation to an identical position in muscovite would consist of two $\frac{a}{2}[110]$ translations, because the octahedrally coordinated Al atoms are ordered (not shown in the figure). However, since the binding energy between the neutral multilayers is weak, the energy minimum associated with $|\mathbf{b}| = \frac{a}{2}[110]$ probably approaches that of the perfect dislocation. It is therefore most conservative to consider $|\mathbf{b}| = \frac{a}{2}[110]$ for both micas, since all the implications considered below for $b = \frac{a}{2}[110]$ are valid for $\mathbf{b} = a[110]$. The dislocation can dissociate into a set of

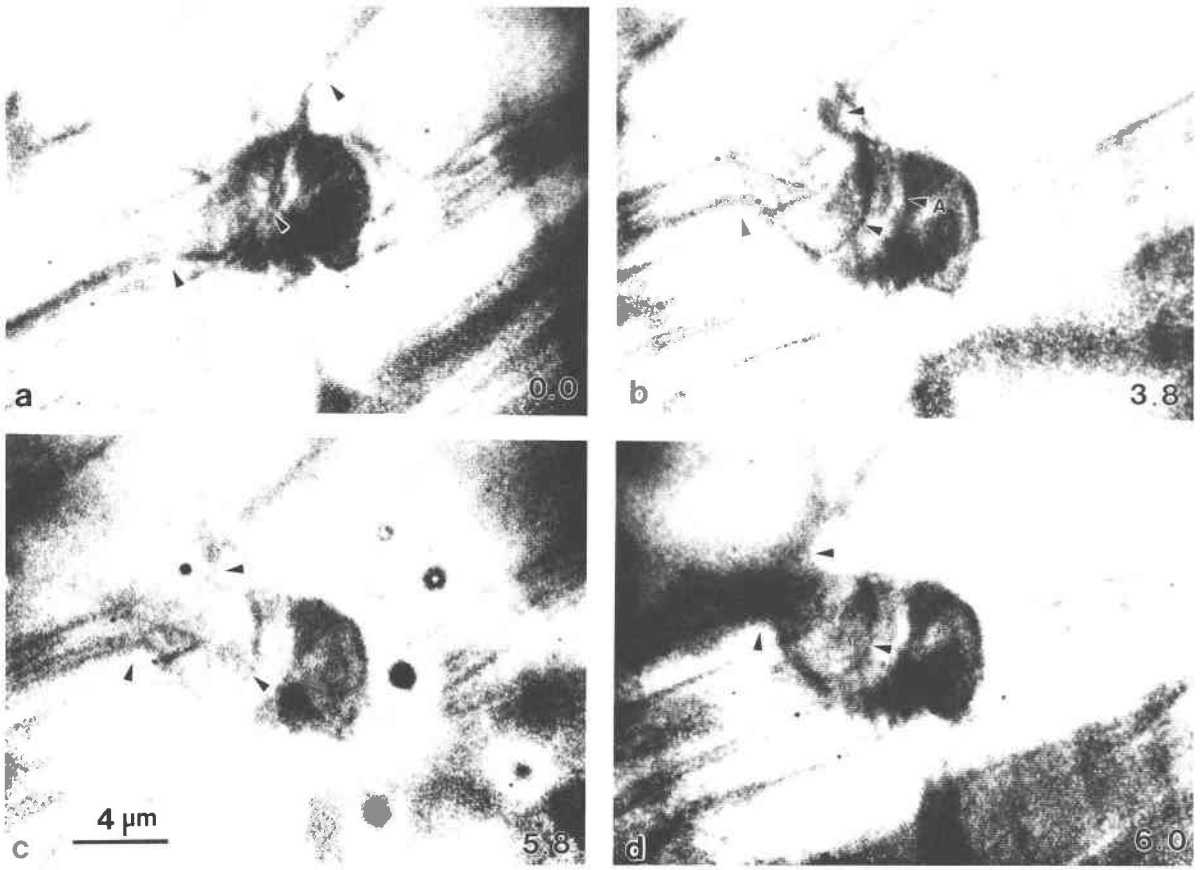

Fig. 10. Bright-field sequence photographed from a videotape of the interaction of a dislocation line with a precipitate in biotite. (**a**) The original positions of a dislocation and a large (~5–6 μm) precipitate. Subsequent movements can be compared to the stationary precipitate. (**b**) The unmarked arrows indicate the advance of the dislocation. The dislocation changes the contrast of the area it traversed, which indicates that it cut a coherent precipitate. Arrow A indicates the original (0.0 min) location of the dislocation line. (**c**) Small particles from specimen breakage elsewhere in the foil burn in a bright burst of fireworks and subsequently leave the dark spots represented in this photomicrograph. (**d**) Beyond a critical radius (~4 μm), the dislocation line attempted to neck rapidly. The Orowan mechanism was unsuccessful, up to the limit of the strain stage.

small steps to nonequivalent positions that are local potential-energy minima ($\mathbf{b} \rightarrow \mathbf{b}_1 + \mathbf{b}_2$). The number of partial dislocations equals the steps in the completed translation. The dissociations proposed here (Table 1) (Fig. 13) are twofold, on the basis of the observed separation of a dislocation into two lines. Partial dislocations for biotite are $\frac{a}{2}[110] \rightarrow \frac{a}{6}[310] + \frac{a}{3}[010]$, $\frac{a}{2}[\bar{1}10] \rightarrow \frac{a}{6}[310] + \frac{a}{3}[010]$, and $a[100] \rightarrow \frac{a}{6}[3\bar{1}0] + \frac{a}{6}[310]$. The indices of the more distorted muscovite structure (Fig. 13) are designated in terms of the structurally equivalent biotite indices. These dissociated pairs differ only slightly from $\frac{a}{4}[110] + \frac{a}{4}[110]$, a doublet version of the fourfold dissociation proposed for trioctahedral talc (Amelinckx and Delavignette, 1962). That difference is insignificant to the present assessment of the Peierls stress. The present choice of partial Burgers vectors agrees with those of Bell and Wilson (1981). In addition, it underscores the structural difference between the dioctahedral and trioctahedral structures, with which Amelinckx and Delavignette were not concerned.

The total energy of a dislocation is directly proportional to $|\mathbf{b}|^2$ (Nabarro, 1967, p. 197). Therefore, although the energy of a perfect dislocation is minimized for shortest translation to an identical position, the energy of the system can be further reduced by dislocation dissociation. The well-known criterion that dislocations dissociate if $|\mathbf{b}_1|^2 + |\mathbf{b}_2|^2 < |\mathbf{b}|^2$ is employed in Table 1 to evaluate the Burgers vectors in muscovite and biotite. On the basis of this criterion, each dissociated pair of biotite appears to be favored over the undissociated dislocation, and all three appear to be energetically equivalent. In muscovite also, all three partial combinations appear to require less energy than the full dislocation. However, $\frac{a}{2}[110] \rightarrow \frac{a}{6}[310] + \frac{a}{3}[010]$, partial combination (a) (Table 1) parallel to the most favored dislocation-line direction (Fig. 12), requires the least energy. As an interesting result of the dioctahedral distortion, this dissociation reaction most closely approximates the partial dissociation proposed by Amelinckx and Delavignette (1962).

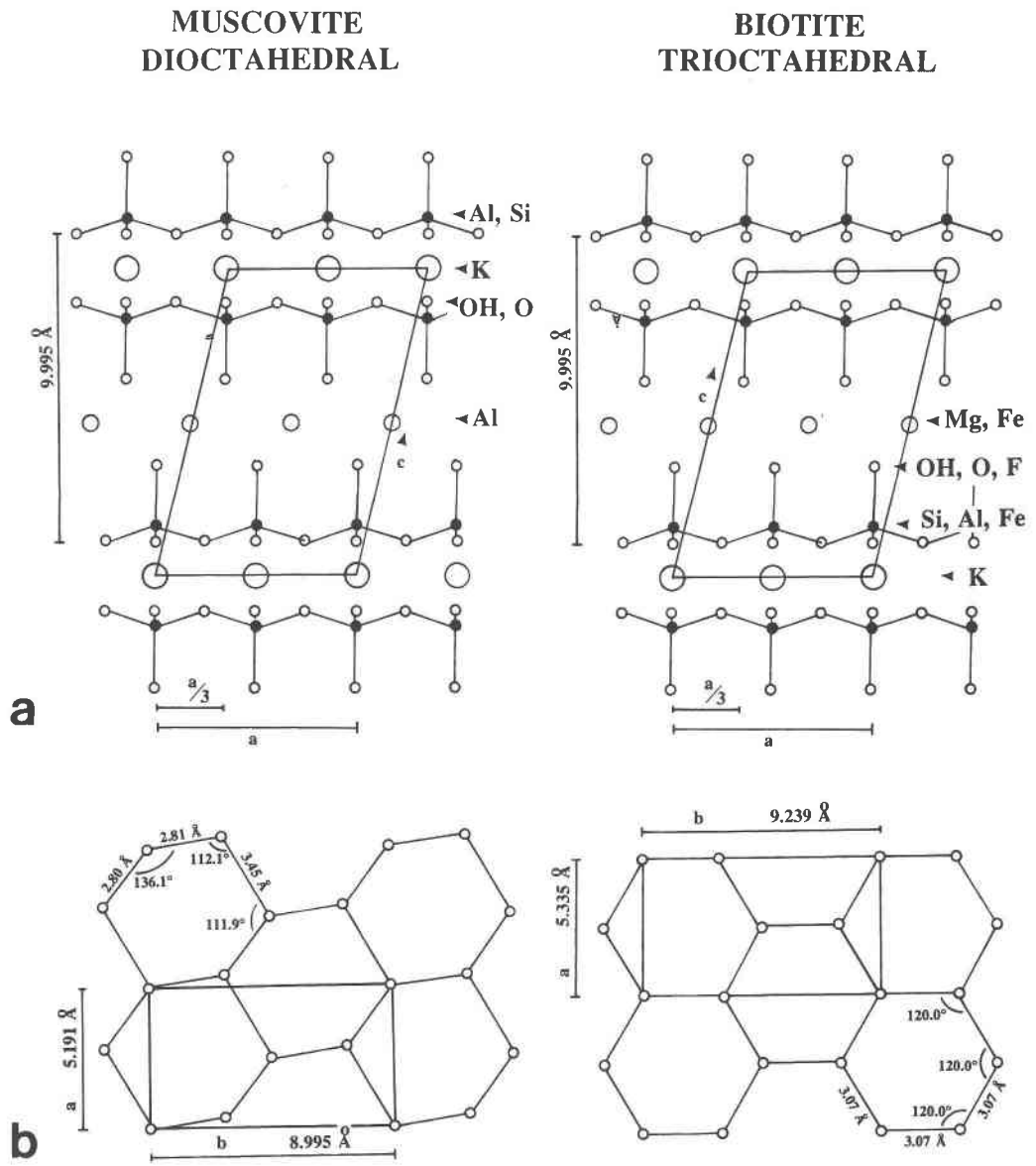

Fig. 11. (**a**) Diagrams of muscovite and biotite viewed parallel to the *b* axis. The fundamental unit cell (outlined) can be stacked in a variety of polytypes. After Deer et al. (1975). (**b**) The view normal to (001) is represented as a diagram of the apical oxygens of a tetrahedral layer in an octahedral sheet. The relative distortion of the dioctahedral sheet is due to the vacancy in one out of every three octahedral sites. After Bailey (1984).

Qualitative illustrations of Peierls potential-energy distributions for basal dislocations provide a useful basis for a comparison between the two micas (Fig. 14). Dislocations influenced by a dioctahedral layer are predisposed toward [110] orientation to each multilayer and thus toward [110] and [100] in a $2M_1$ polytype. The undissociated Burgers vectors $\frac{a}{2}[110]$, $\frac{a}{2}[\bar{1}10]$, and $a[110]$ are nearly identical, but if dissociated, the favored [110] reaction would give the dislocations screw character. These considerations suggest that muscovite favors screw dislocation as a function of the role dissociation plays in dislocation activation and, further, dissociation is important under the experimental conditions. Basal dislocations influenced by a trioctahedral layer favor [100], [110], and $[\bar{1}10]$ equally within one multilayer and can thus take up a curvilinear habit. Biotite dislocations can take on either character, since all dissociation reactions are favored equally and both parallel and normal Burgers vectors can be found for any potential dislocation line. However, in view of the frequently observed phenomenon that edge dislocations often achieve higher velocities, sometimes 50 times faster, than screw dislocations (Kabler, 1963;

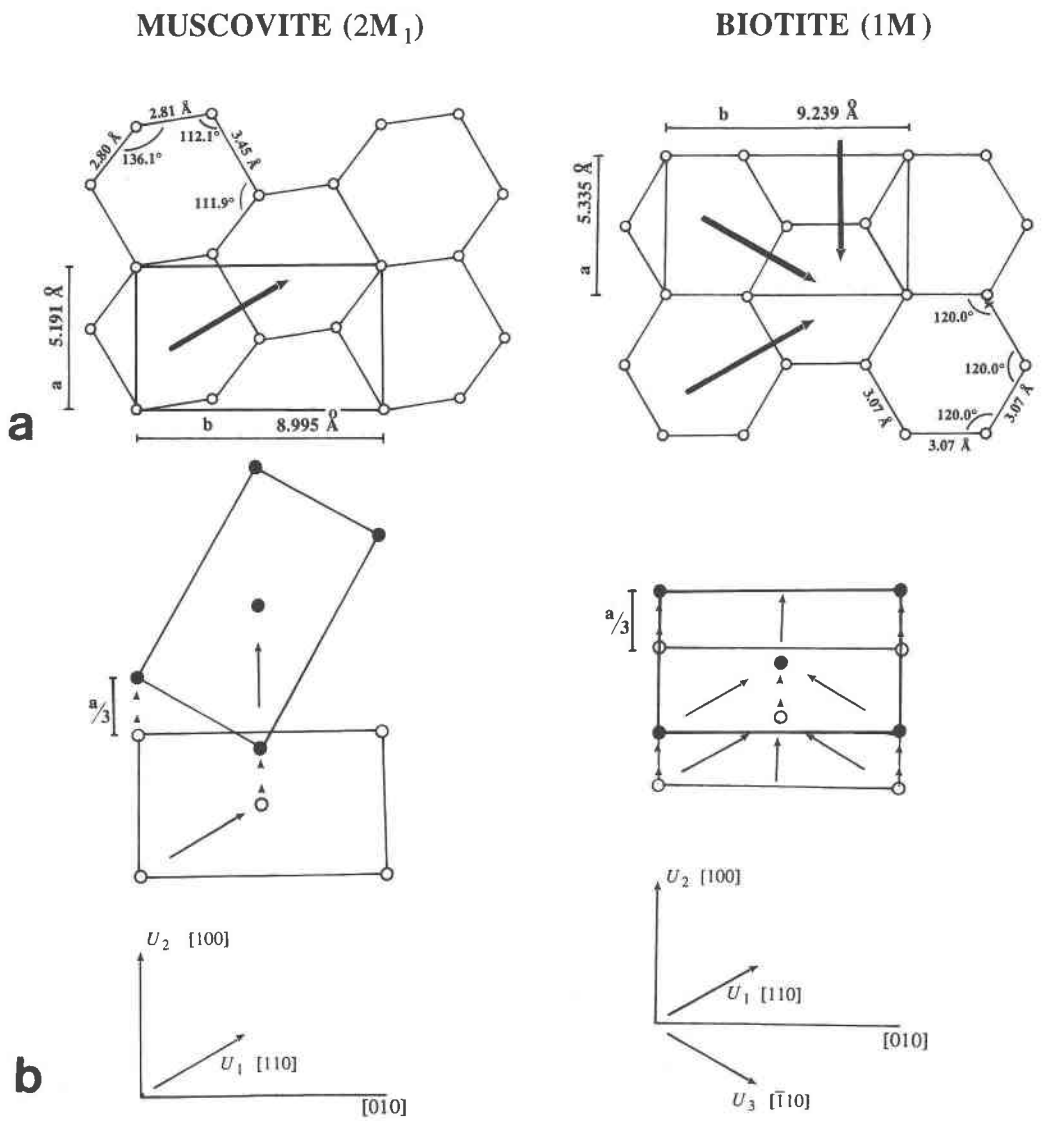

Fig. 12. (**a**) The influence of octahedral sheets, represented as in Fig. 11b, on the orientation of unstressed dislocations (dark lines). A trioctahedral sheet would give equal preference to the symmetrically equivalent [100], [110], and [1̄10] orientations. A dioctahedral sheet would give preference to the [110] orientation. (**b**) The effect of polytypic stacking on dislocation orientation. Alternate layers of the $2M_1$ polytype are translated and rotated 30°. Consequently, the [110] of one layer is equivalent to the [100] of the adjacent layer. The $1M$ polytype stacking sequence does not affect the dislocation orientation.

Celli et al., 1963), one might expect the faster-moving edge dislocations when the structure allows, as is observed in the biotite specimens.

A strict comparison between screw and edge dislocations is only allowed for dislocations in the same material, where it has a sound basis in energetic arguments (Weertman and Weertman, 1980). However, one is also tempted to seek an explanation for the velocity difference between dislocation in muscovite and biotite. A comparison of structurally similar but chemically distinct materials also requires consideration of "solute drag," in which a dislocation must escape from a solute "atmosphere" (Hirth and Lothe, 1968, p. 584–633). Consequently, the identity of the atoms can affect the dislocation velocity. As a further complication, the stress field about the screw dislocation allows solute drag to affect its velocity to a greater extent (e.g., Schöck, 1980). The present arguments invoke the standard assumption, based on the strength of interlayer bonds, that the glide plane is located between multilayers (Amelinckx and Delavignette, 1962). In that case a muscovite dislocation would encounter nothing chemically different than a biotite dislocation. The muscovite dislocation would only experience a relative shift in the placement of K atoms because

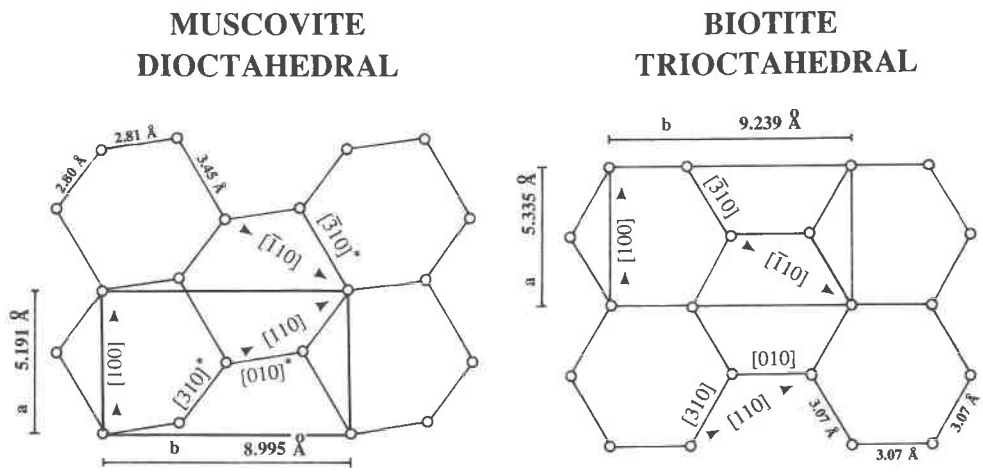

Fig. 13. An illustration of the partial Burgers vector evaluated in Table 1, represented as in Fig. 11b.

of the octahedral distortion. If basal slip was located within the octahedral layer, as has been proposed for growth defects (Bell and Wilson, 1977), further discussion of the effects of temperature, atomic radius, and charge would be necessary. For these preliminary results, however, the structural arguments lead directly to dislocations of a character consistent with the observed velocity difference, and it is unnecessary to appeal to solute drag.

The videotaped sequence in which the biotite dislocation left a loop behind upon relaxation to an earlier position (Fig. 9) suggested that the stressed dislocation reached a potential well. The further implication that Peierls stress was significant under the experimental conditions compared favorably with an earlier model for dislocation mobility in semiconductors (Celli et al., 1963). In that model, low-stress dislocation activation was distinguished from high-stress dislocation activation, in which the dislocation would remain on the crest of the Peierls potential-energy surface. Certainly the complex relationships between deformation conditions and dislocation mobility are not completely understood. For example, linear basal dislocations have been observed in trioctahedral talc (Amelinckx and Delavignette, 1962). However, the present observations and their agreement with energetic considerations suggest some optimism toward the eventual ability to predict these relationships. Furthermore, one can take advantage of the dependence of dislocation activity on deformation conditions to test the present proposal. Differences controlled by Peierls stress should decrease as temperature increases and thermal vibrations mask its effects. Therefore, if the present proposal is valid, then the difference between dislocation activity in muscovite and biotite should disappear with increasing temperature and perhaps with increasing stress. The existence of this variation has not been verified but may be corroborated by observations from naturally deformed specimens.

Image contrast and dislocation dynamics

A rigorous Burgers vector analysis is complicated under the most benevolent circumstances in an anisotropic material. The standard isotropic invisibility criteria are $\mathbf{g} \cdot \mathbf{b} = 0$ for all dislocations, and $\mathbf{g} \cdot \mathbf{b} \times \mathbf{u} = 0$ for edge dislocations, owing to displacements normal to the dis-

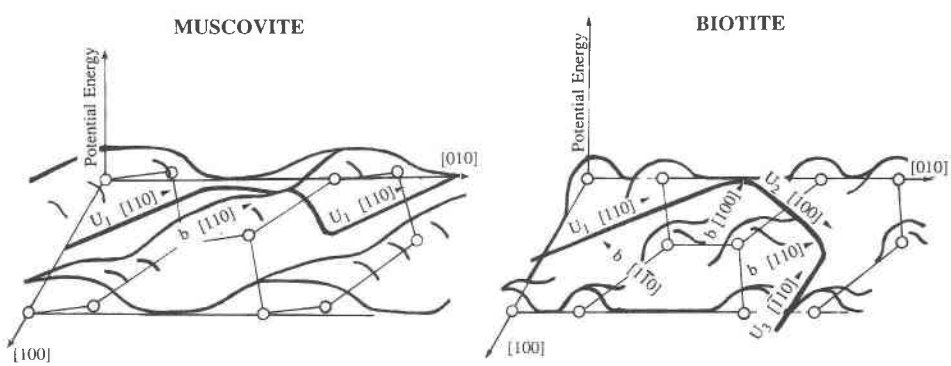

Fig. 14. A diagram of the Peierls potential-energy distribution in the octahedral layer. (a) Muscovite dislocations will tend to lie in straight segments and prefer screw character. (b) Biotite dislocations can be curvilinear and can take on edge character.

TABLE 1. A summary of $|\mathbf{b}_1|^2 + |\mathbf{b}_2|^2$ and $|\mathbf{b}|^2$ for the evaluation of dislocation dissociation reactions

	(a)	(b)	(c)	(d)
Burgers vector	$\frac{a}{6}[310] + \frac{a}{3}[010]$	$\frac{a}{6}[\bar{3}10] + \frac{a}{3}[010]$	$\frac{a}{6}[3\bar{1}0] + \frac{a}{6}[310]$	$\frac{a}{2}\langle 110\rangle$
Biotite	$\|\mathbf{b}_1\|^2 + \|\mathbf{b}_2\|^2 = 18.85$	$\|\mathbf{b}_1\|^2 + \|\mathbf{b}_2\|^2 = 18.85$	$\|\mathbf{b}_1\|^2 + \|\mathbf{b}_2\|^2 = 18.85$	$\|\mathbf{b}\|^2 = 28.46$
Muscovite	$\|\mathbf{b}_1\|^2 + \|\mathbf{b}_2\|^2 = 15.74$	$\|\mathbf{b}_1\|^2 + \|\mathbf{b}_2\|^2 = 19.80$	$\|\mathbf{b}_1\|^2 + \|\mathbf{b}_2\|^2 = 19.80$	$\|\mathbf{b}\|^2 = 26.95$

location line (**u**). Since all the Burgers vectors and dislocation lines of interest were in the (001) glide plane, $\mathbf{g} \cdot \mathbf{b} \times \mathbf{u} = 0$ was satisfied for all $hk0$. However, Head et al. (1967) have shown that these criteria do not apply in general to anisotropic materials, but only to pure edge or screw dislocations oriented normal to a plane of symmetry. Numerical methods are often needed to interpret these more complex cases of image contrast. The isotropic invisibility criteria are adopted for this preliminary assessment, under the assumption that residual contrast was low if low-order reflections were used. The screw character of muscovite dislocations, determined from comparison with isotropic invisibility criteria, was consistent with the observed dislocation activation as well as the energy-minimization arguments. Similar $\mathbf{g} \cdot \mathbf{b}$ analyses of dislocations in biotite indicated that the leading edge of the bowed dislocations had edge character, which was strictly consistent with the dislocation-velocity experiments cited earlier.

Images from a typical Burgers vector determination in a muscovite specimen are illustrated in Figure 6. Dislocations oriented in [100] and [110] are most easily observed in Figure 6a. Some of the dislocation lines crossed but did not appear to be affected by the presence of the other line. This apparent independence indicated that the dislocations inhabited multiple glide planes and, as a result, that the images may suffer from interfering contrast. The dark bands on the lower left side of Figure 6d and the [110]-oriented bands in the upper left corner (Fig. 6b) were interpreted as stacking faults and will be discussed in more detail below. The [110] dislocation images that showed no bands of reversed contrast were only invisible for $\mathbf{g} = 1\bar{1}0$. Comparison of these apparently complete [110]-oriented dislocations with the values of $\mathbf{g} \cdot \mathbf{b}$ for the reflections in Figure 6 (Table 2) suggested that the Burgers vector is $\frac{a}{2}[110]$. The general trend of contrast intensities for the first class of [100]-oriented dislocations, those that were least visible for $\mathbf{g} = 1\bar{1}0$, was consistent with an $a[100]$ Burgers vector. Therefore both perfect [100]- and [110]-oriented dislocations were identified as screw dislocations.

TABLE 2 A summary of $\mathbf{g} \cdot \mathbf{b}$ values for reflections from Fig. 6 and perfect $\frac{a}{2}\langle 110\rangle$ dislocations

	b		
g	$\frac{a}{2}[110]$	[100]	$\frac{a}{2}[\bar{1}10]$
(a) $1\bar{3}0$	−1	1	−2
(b) $1\bar{1}0$	0	1	−1
(c) 200	1	2	−1
(c) 110	1	1	0
(d) 020	1	0	1

As discussed in the previous section, the distinction between perfect and partial dislocations has significant energetic ramifications. The observed division of single dislocation lines was interpreted as the result of dislocation dissociation. The dislocations in both muscovite and biotite that split into two lines separated by an area of either reduced or unchanged image intensity were considered twofold dissociations. In the absence of evidence of further dissociation that might be expected from earlier observations of talc (Amelinckx and Delavignette, 1962), this conservative approach was adopted. Moiré fringes in biotite were associated with three or more dislocation lines and will be treated separately. The structure-factor argument below is presented to demonstrate that the previously suggested partial dislocations could create a stacking fault that exhibited either reversed or unchanged contrast. But this section also demonstrates the potential complexity of an image of superimposed partial dislocations.

Image intensity is an inverse Fourier transform of the intensity $(F_{hkl})^2$ of the diffracted beam hkl (e.g., Cowley, 1984). The discussion of the structure factor (F_{hkl}) below is limited to two-beam imaging conditions. Only $hk0$ reflections are considered since the beam direction remained subparallel to [001] during the experiment. The structure factor for the undeformed crystal can be described in the following manner:

$$F_{hk0} = \sum_m f(\Theta)_m \exp[2\pi i(x_m h + y_m k)] + \sum_o f(\Theta)_o \exp[2\pi i(x_o h + y_o k)], \quad (1)$$

where atoms designated m and o are divided by the (001) slip plane. After an $\frac{a}{2}[110]$ dislocation sweeps through the crystal, the second exponential takes the form $\exp\{2\pi i[(x_o + \frac{1}{2})h + (y_o + \frac{1}{2})k]\}$. If $h + k$ is even, F_{hk0} is identical to Equation 1, and the contrast will not be affected. If $h + k$ is odd, the second exponential is negative, and F_{hk0} is reduced in the area swept by the dislocation. But odd $h + k$ reflections are not allowed for either $1M$ biotite or $2M_1$ muscovite. Therefore, even though Burgers vectors of $\frac{a}{2}[110]$ and $[\bar{1}10]$ are indistinguishable on the basis of

image contrast, the reversed contrast in muscovite could not be due to the twofold combination $\frac{a}{2}[110] + \frac{a}{2}[1\bar{1}0] = a[110]$. Minimum-energy considerations also suggest that this latter possibility is unlikely. Note that this and the following simple contrast interpretations do not distinguish between a dislocation with a Burgers vector **b** and a "superdislocation" with a Burgers vector **x** + **b**, where |**b**| is less than one unit-cell length and |**x**| is an integer multiple of a unit-cell length in the direction of the Burgers vector. In this first interpretation of dynamic observations, it has not been necessary to invoke superdislocations. Although they may have significant implications in the future, they are not within the scope of this paper.

Partial dislocations could have been responsible for the reversed contrast between split dislocations. The displacement vector (**R**) due to a stacking fault is usually not identical to the partial Burgers vector of the dislocation that has swept the area because the atomic bonds compensate for the new nearest neighbors (e.g., Thomas and Goringe, 1979). The Burgers vector is used below to approximate **R** for three reasons. First, since only *hk*0 reflections are considered, expansion or contraction parallel to [001] can be ignored. It is valid to assume that the component of **R** resolved onto (001) ($\mathbf{R}_{(001)}$) was reasonably close to **b**. Second, the stacking-fault displacements were not determined in the interest of making more general preliminary observations of the interaction between dislocations and precipitates. The determination of a stacking-fault displacement is a standard experimental technique, but it takes several minutes to perform and an exhaustive evaluation can last much longer. Since the technique involves extensive use of diffraction patterns, the video camera must be turned off, which was unacceptable in this dynamic case where the stacking faults appeared for a few seconds to a minute. Third, these displacements agree with those determined previously by Bell and Wilson (1981).

Consider a stacking fault in biotite with a resolved displacement $\mathbf{R}_{(001)} \approx [a/2\ a/6\ 0]$:

$$F_{hk0} = \sum_m f(\Theta)_m \exp[2\pi i(x_m h + y_m k)] + \sum_o f(\Theta)_o \exp[2\pi i(x_o h + y_o k)] \cdot \exp[\pi i(h + \tfrac{1}{3}k)]. \quad (2)$$

For some reflections F_{hk0} remains constant. However, for other allowed reflections the third exponential, $\exp[\pi i(h + \frac{1}{3}k)]$, can approach -1 and reduce the value of F_{hk0}. Arguments are identical for the other partial dislocations (b) and (c) (Table 1) and notably also for the dissociated dislocation: $\frac{a}{4}[110] + \frac{a}{4}[1\bar{1}0]$. The potentially higher-order displacement vectors of muscovite would have similar effects on image contrast. Therefore the dislocation lines that separated and left the contrast unchanged, observed primarily in muscovite (Fig. 5), were probably not the perfect dislocations $\frac{a}{2}[110] + \frac{a}{2}[1\bar{1}0]$ discussed above, but rather stacking faults imaged under conditions for which F_{hk0} was unaffected (e.g., $h + k/3$ is even). This phase shift ($\alpha = 2\pi\mathbf{g} \cdot \mathbf{R}$), which describes stacking-fault contrast, is employed below to identify the partial dislocations responsible for the dark gray bands in Figures 6b and 6d.

Table 3 lists **g** • **b** values for the reflections represented in Figure 6, partial dislocations, and the phase shift (α). For the dislocation line, **g** • **b** $\leq \frac{2}{3}$ was considered invisible in many cases, which is not unusual for an anisotropic crystal (Clarebrough, 1971). A phase shift, $\alpha \leq \pi/3$ was considered invisible for a stacking fault, in strict agreement with standard practice for isotropic crystals (Thomas and Goringe, 1979, p. 161–164). Comparison of image contrast with the values listed in Table 3 suggested the dissociation reaction $\frac{a}{2}[110] \rightarrow \frac{a}{6}[310] + \frac{a}{3}[010]$ for the [110]-oriented dislocations. The presence of stacking-fault contrast for $\mathbf{g} = 1\bar{1}0$ but not for $\mathbf{g} = 020$ suggested that $\mathbf{R} = \frac{a}{3}[010]$. The thin [100]-oriented lines of low contrast for $\mathbf{g} = 020$ (Figs. 6c and 6d) were invisible for $\mathbf{g} = 1\bar{3}0$ (Fig. 6a), but had strong contrast for $\mathbf{g} = 110$ (Fig. 6c). The white lines could be further associated with the stacking-fault contrast in Figure 6d. Comparison with Table 3 suggested the dissociation reaction $\frac{a}{6}[310] + \frac{a}{6}[3\bar{1}0]$. The stacking-fault contrast appeared for $\mathbf{g} = 020$ and was invisible for $\mathbf{g} = 1\bar{1}0$, which suggested that **R** is $\frac{a}{6}[3\bar{1}0]$. According to the Burgers vector analysis, both the [100]- and the [110]-oriented dissociated dislocations also had screw character. The further implication that two glide planes of [100]-oriented screw dislocations were superimposed was consistent with the bold moiré fringes for $\mathbf{g} = 1\bar{1}0$ (Fig. 6c). Such interfering contrast would be expected where **g** • **b** was nonzero for both one partial dislocation and the stacking fault of the dissociated dislocation and the superimposed perfect dislocation.

Images of the advancing biotite dislocations were often diffuse (Fig. 8), which may have been due in part to the depth of the dislocation in the foil. However, at higher magnification, it appeared that these were dissociated dislocations. Dislocations in biotite dissociated readily to widths of approximately 0.1 to 0.5 μm. Since dislocations are known to be elastic, one might expect to observe wider stacking faults in dynamic experiments than under static conditions. The frequency with which dislocations seemed to dissociate when confronted by obstacles was more of a surprise. Two examples of dislocation dissociation involved foil-normal dislocations in one case (Fig. 4a) and a large precipitate in the other (Fig. 9). Shorter Burgers vectors and more suitable vector directions may have lowered the passing stress. The potential for dissociations also may have depended on the distance between pinpoints, which were the edges of the precipitate in the latter case. These contributions were probably more significant under cold working conditions than they are at higher temperatures.

Moiré fringes are caused by a slightly disharmonic spacing or rotation between two parts of a crystal (Bassett et al., 1958). The moiré fringes observed in biotite (Fig. 7) appeared to be associated with dislocation loops and

TABLE 3. A summary of **g•b** values for reflections from Fig. 6 and dissociated dislocations

	$\frac{a}{3}[310]$		$\frac{a}{3}[010]$		$\frac{a}{3}[3\bar{1}0]$		$\frac{a}{3}[0\bar{1}0]$	
g	g•b	α	g•b	α	g•b	α	g•b	α
(a) $1\bar{3}0$	0	0	−1	0	1	0	1	0
(b) $11\bar{1}0$	1/3	$2\pi/3$	−1/3	$-2\pi/3$	2/3	$\pi/3$	1/3	$2\pi/3$
(c) 200	1	0	0	0	1	0	0	0
(c) 110	2/3	$\pi/3$	1/3	$2\pi/3$	1/3	$2\pi/3$	−1/3	$-2\pi/3$
(d) 020	1/3	$2\pi/3$	2/3	$\pi/3$	−1/3	$-2\pi/3$	−2/3	$\pi/3$

were therefore believed to be a consequence of a misfit between the the slipped surfaces of the crystal. The difference between the moiré fringes and the reverse contrast described above could be due to specimen tilt. The local strain about the partial dislocations (a), (b), and (c) (Table 1), similar to that associated with similar partial dislocations in graphite (Amelinckx and Delavignette, 1962, p. 311), could have created a moiré fringe effect if viewed at an angle subnormal to the (001). However, two factors suggested the existence of a second type of dissociation. First, the local strain illustrated by Amelinckx and Delavignette may not influence an area great enough to explain the width of the moiré patterns (>4 μm) represented in Figure 7. Second, the presence of moiré fringes inside the second of the concentric partial loops (Fig. 7) suggested that the dissociation involved at least three partial dislocations. These moiré fringes may have been due to fourfold dissociation discussed by Amelinckx and Delavignette (1962, p. 302)

Despite the relative abundance of potential obstacles in the biotite specimens, biotite dislocations were easier to activate than those of muscovite. Therefore, in these room-temperature experiments, the difference between the stresses required to activate screw and edge dislocations would seem to outweigh the defect pinning effects. The single case of slow activation cited earlier may be explained by activation in an area of lower resolved stress, since dislocation velocity is a function of normalized excess stress (Gilman, 1960). This explanation was supported by the observation that beyond a critical radius, when the line tension became very high, the necking occurred in the rapid manner typical of biotite. However, two other distinctions could be made between these conditions and those in which rapid activation was observed. First, the precipitate was very large. Second, the dislocation did not appear to separate at any point other than across the boundary between the precipitate and the mica. The reversed contrast is interpreted as a dissociation reaction undertaken to cut a coherent precipitate.

The concentric loops observed in biotite (Fig. 8) are currently interpreted as Orowan loops. This interpretation is consistent with the repeated successful operation of the Orowan mechanism that would be expected of dislocation movement through a field of precipitates. These discontinuities and those that resulted from a relaxation mechanism (Fig. 9) increased the number of potential obstacles in biotite. However, they did not appear to affect dislocation mobility. The foil-normal dislocations presented only a slight impediment to basal slip, but did not activate, consistent with the stress geometry of the modified specimen assembly. The greater curvature of the basal dislocation line at the planar defects suggested that the planar defects were more effective pinpoints than the foil-normal dislocations. The jogs in (001) dislocations (Fig. 7) suggested that the planar defects were stacking faults, not the boundary between two halves of a kink. The observed (001) dislocations moved parallel to the planar defects. However, given the appropriate shear-stress orientation, the planar defects are a potential source of greater ductility. Cross-slip could have occurred, and the foil-normal planar defects could have acted as Frank-Read sources (Frank and Read, 1950). The Frank-Read mechanism, however, has not yet been observed in the present experiments.

SUMMARY AND CONCLUSIONS

Basal slip was successfully activated in muscovite and biotite deformed in situ in a high-voltage transmission electron microscope. This work represents the first results of ongoing experiments. In view of the novelty of the approach to geologic applications, more general observations and image interpretation have been emphasized. In these specimens, muscovite dislocations are distinguished from biotite dislocations by their extreme length, linearity, and screw character. Even though the biotite specimens contained more obstacles to dislocation movement, the biotite dislocations were more mobile than the muscovite dislocations. The distinctness of the difference between such similar mica structures was unexpected. However, the observation is consistent with differences inferred from static observation (Bell and Wilson, 1981). The twofold dissociation reaction that seems to predominate in biotite is usually associated with obstacle encounters. An apparently fourfold dissociation in biotite, although seldom observed, seems unrelated to the circumvention of obstacles. The muscovite specimens were free of obstacles, but all the dissociation reactions appeared to be twofold.

In view of the differences that were observed, a working hypothesis for future study has been developed. Under

the assumption that solute drag can be ignored, the experimentally observed differences in dislocation mobility exhibited by the two mica specimens seem to reduce to the differences between edge and screw dislocations. The relative rapidity of an edge dislocation and the number of low-energy mechanisms at its disposal to activate new dislocations and to circumvent obstacles are consistent with these observations. This would suggest that under the experimental conditions, the character of dislocations could have more influence on the macroscopic ductility than the presence of obstacles.

The general micromechanical differences between these mica specimens are consistent with the slightly greater anisotropy of the dioctahedral sheet silicate and consequently that of the Peierls potential-energy distribution. Review of the structures suggests that muscovite is more restricted to screw dislocations whereas biotite can take either character and can therefore take advantage of the more rapid edge character. One would expect these simple structural considerations to be less consistent with observed behavior if more than one slip plane is involved, or if there is a greater potential for climb. However, the proposal establishes a context for further study of the micas. Peierls stress control of dislocation activity implies that the observed characteristics should be influenced by deformation conditions. An investigation into the effects of temperature on the difference in dislocation activity would be an appropriate test of this interpretation.

The results of this comparative study of biotite and muscovite are evidence of the utility of the in situ experimental approach. The advantage of in situ experiments is the ability to observe dynamic and nonequilibrium interactions. The experimental observations have especially significant ramifications for the understanding of cold-working behavior. The dislocation dissociations observed during interactions with obstacles in these experiments are not preserved for static observation and are not necessarily predictable from physical measurements such as stacking-fault energies that are determined from static observations. In situ experiments performed on these nonmetallic anisotropic materials also provide a valuable comparison to the better-known behavior of dislocations in metals.

Acknowledgments

I would like to thank R. Gronsky, W. D. Means, R. Reeder, H.-R. Wenk, and an anonymous reviewer for helpful comments and reviews of the manuscript. Use of the HVEM at the National Center for Electron Microscopy, Lawrence Berkeley Laboratory, Berkeley, California, is gratefully acknowledged. Support for this work was furnished in part by a University of California President's Postdoctoral Fellowship and U. S. Department of Energy Contract No. DE-AC03-76SF00098.

References cited

Abbott, R.N., and Burnham, C.W. (1988) Polytypism in micas: A polyhedral approach to energy calculations. American Mineralogist, 73, 105–118.

Amelinckx, S., and Delavignette, P. (1962) Dislocations in layered structures. In J.B. Newkirk and J.H. Wernick, Eds., Proceedings, Technical Conference on Direct Observation of Imperfections in Crystals, Missouri, p. 295–356. Wiley, New York.

Bailey, S.W. (1984) Classification and structures of the micas. Mineralogical Society of America Reviews in Mineralogy, 13, 1–13.

Bassett, G.A., Menter, J.W., and Pashley, D.W. (1958) Moiré patterns on electron micrographs. Royal Society London Proceedings, Series A, 246, 345–368.

Bell, I.A., and Wilson C.J. (1977) Growth defects in metamorphic biotite. Physics and Chemistry of Minerals, 2, 153–169.

——— (1981) Deformation of biotite and muscovite: TEM microstructure and deformation model. Tectonophysics, 78, 201–228.

Campany, R.E., Loretto, M.H., and Smallman, R.E. (1976) Dynamic observation during tensile deformation of molybdenum in the high voltage electron microscope. Metal Science, 10, 253–259.

Celli, V., Kabler, M., Ninomiya, T., and Thomson, R. (1963) Theory of dislocation mobility in semiconductors. Physical Review, 131, 58–72.

Clarebrough, L.M. (1971) Contrast from Shockley partial dislocations. Australian Journal of Physics, 24, 79–96.

Cowley, J. (1984) Diffraction physics (2nd revised edition). North-Holland Publishing, Amsterdam.

Deer, W.A., Howie, R.A., and Zussman, J. (1975) An introduction to the rock-forming minerals. Longman Group, London.

Etheridge, M.A., Hobbs, B.E., and Paterson, M.S. (1973) Experimental deformation of single crystals of biotite. Contributions to Mineralogy and Petrology, 38, 21–36.

Frank, F.C., and Read, W.T. (1950) Multiplication processes for slow-moving dislocations. Physical Review, 79, 722–723.

Frank, F.C., and van der Merwe, J.H. (1949) One-dimensional dislocations. I. Static theory. Royal Society London Proceedings, Series A, 198, 205–216.

Franks, F. (1984) Atom beam source. Vacuum, 34, 259–261.

Gerold, V. (1983) Precipitation hardening. In F.R.N. Nabarro, Ed., Dislocations in solids, vol. 4: Dislocations in metallurgy (2nd edition), p. 219–260. North Holland Publishing, New York.

Gilman, J.J. (1960) The plastic resistance of crystals. Australian Journal of Physics, 13, 327–343.

Head, A.K., Loretto, M.H., Humble, P. (1967) The influence of large elastic anisotropy on the determination of Burgers vectors of dislocations in β-brass by electron microscopy. Physica Status Solidi, 20, 505–519.

Hirth, J.P., and Lothe, J. (1968) Theory of dislocations. McGraw Hill, New York.

Imura, T., and Hashimoto, H., Eds. (1977) Proceedings of the Fifth International Conference on High Voltage Electron Microscopy, Kyoto, Japan (supplement of Journal of Electron Microscopy).

Kabler, M.N. (1963) Dislocation mobility in germanium. Physical Review, 131, 54–58.

Meike, A. (1988) Specimen cage modification for TEM in situ shearing. In J.C. Bravman, R.M. Anderson, and M.L. McDonald, Eds., Specimen preparation for transmission electron microscopy of materials, Materials Research Society Symposium Proceedings, 115, 211–216. Materials Research Society, Pittsburgh, Pennsylvania.

Messerschmidt, U., and Appel, F. (1979) Method of evaluating geometrical-statistical parameters of the interaction between dislocations and point obstacles from electron micrographs. Kristall und Technik, 14, 1331–1337.

Mügge, O. (1898) Ueber Translationen und verwandte Erscheinungen in Kristallen. Neus Jahrbuch für Mineralogie, Geologie und Paläontologie, 1, 71–158.

Nabarro, F.R.N. (1967) Theory of dislocations. Oxford University Press, London.

Orowan, E. (1954) Dislocations and mechanical properties. In M. Cohen, Ed., Dislocations in metals, p. 69–195. American Institute of Mining and Metallurgical Engineers, New York.

Peierls, R. (1940) The size of a dislocation. Proceedings of the Physical Society of London, 52, 34–37.

Richter, U., Ed. (1979) Proceedings of the international symposium, in-situ high voltage electron microscopy: Application to plasticity and further topics of materials research. Kristall und Technik, 14, 1171–1417.

Schöck, G. (1980) Thermodynamics and thermal activation of disloca-

tions. In F.R.N. Nabarro, Ed., Dislocations in solids, vol. 3: Moving dislocations, p. 63–164. North Holland Publishing, New York.
Thomas, G., and Goringe, M.J. (1979) Transmission electron microscopy of materials. Wiley, New York.
Van der Biest, O., and Thomas, G. (1976) Fundamentals of electron microscopy. In H.-R. Wenk, Ed., Electron microscopy in mineralogy, p. 18–51. Springer-Verlag, New York.
Weertman, J., and Weertman, J.R. (1980) Moving dislocations. In F.R.N. Nabarro, Ed., Dislocations in solids, vol. 3: Moving dislocations, 1–61. North Holland Publishing, New York.

Manuscript received October 18, 1988
Manuscript accepted March 16, 1989